Optical Binding Between Knotted and Chiral Nanoparticles

Stephen H. Simpson[a] and Simon Hanna[b]

[a]Institute of Scientific Instruments of the ASCR, v.v.i., Královopolská 147, 612 64 Brno, Czech Republic

[b]H.H. Wills Physics Laboratory, University of Bristol, Tyndall Avenue, Bristol BS8 1TL, UK

ABSTRACT

Optical binding occurs when systems of both dielectric particles are illuminated by intense light fields, and results in the formation of clusters and coupled dynamical behaviour. Optical binding between spheres has been studied extensively, but little has appeared in the literature describing binding in lower symmetry systems. Here we discuss computer simulations of optical binding between hypothetical knotted nanowires. The knots chosen are drawn from the class of knots known as torus knots which may be represented with n-fold chiral rotational symmetry. We examine the binding properties of the knots in circularly polarised counter propagating beams.

Keywords: Optical binding, counter-propagating plane waves, knotted nanowires, torus knots, computer simulation, coupled dipole method

1. INTRODUCTION

Since the phenomenon of optical binding was first observed, over twenty-five years ago,[1] the phenomenon has been widely studied. Optical binding results from multiple scattering between particles, and can result both in an ordered arrangment of matter[2] and the generation of complex, non-conservative, motion.[3] Most optical binding studies have involved dielectric (e.g. silica) spheres,[4–6] although recent departures from this trend include more strongly bound nanoparticles,[7,8] silver bipyramids[9] and carbon nanotubes.[10] The reduction of particle symmetry introduces further complexity into the system, with ordering involving both positional and orientational degrees of freedom, as well as introducing the possibility of further non-conservative effects.[11] While optical tweezers has been widely applied to the task of nanoparticle manipulation,[12–17] there is increasing interest in techniques for promoting self-organisation.[18,19] Optical binding offers one such possibility.

Although initially appearing to be a mathematical abstraction, knots are becoming ubiquitous across the sciences. They are found in biological molecules, including proteins[20,21] and DNA,[22,23] and are thought to participate in gene regulation,[24] knotted vortices are found in optical speckle patterns,[25] and knots have recently been discussed in the context of tangled quantum wave functions[26] and in the order parameter of a spinor Bose-Einstein condensate.[27]

In the present paper we use knotted nanowires as model chiral particles with which to study optical binding in circularly polarised counter propagating beams. The knotted nanowire is not naturally occurring, but could in principle be fabricated relatively easily using two-photon polymerisation. In this study we present the results of computer simulations of optical binding between knots of differing chiral symmetry. In particular, we focus on the chiral torus knots such as the trefoil (3_1), and cinquefoil (5_1), as well as the 4-fold rotationally symmetric, 8-crossing 8_{19} knot (see Fig. 1).

Further author information: (Send correspondence to S.H.)

S.H.: E-mail: s.hanna@bristol.ac.uk, Telephone: +44 117 928 8771

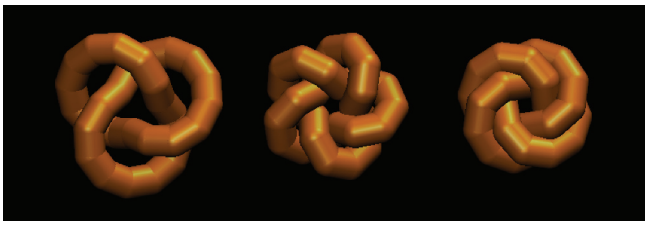

Figure 1. Schematic showing the three knotted nanowires used throughout this paper. In the simulations, the knotted nanowires are oriented so that the faces shown are perpendicular to the propagation direction. i.e. the plane of the diagram corresponds to a bright interference fringe.

2. METHODS

2.1 Computational model

It is assumed that the knotted nanowires are immersed in a viscous medium, such as water. The motion of the bound particles is therefore determined by their hydrodynamic interactions, stochastic forces, as well as optical forces. In the computer model, all the above interactions are included using a coarse-grained approach. The knots are represented by a rigid lines of interacting spheres, each of which act as centres for the hydrodynamic and the optical calculations. The optical, thermal and hydrodynamics forces acting on each bead are calculated in turn. These forces are then used to determine the forces and torques acting on the each knotted nanowire, so that it moves as a rigid body.

The optical interactions are calculated using the coupled dipole method (CDM).[4,28–30] Each knot is decomposed into a collection of dipolar cells, corresponding to the beads, each of which is associated with a point polarizability. The polarisabilities are solved self-consistently using an iterative approach. The force on each bead is then found from the Lorentz force law.[4]

The diffusion matrix for the constituent beads is obtained using either the Oseen or Rotne-Prager tensor.[31] The diffusion matrix for the system of knots is then required. To obtain this, the bead diffusion matrix is inverted, to give a bead friction matrix, from which the forces on all the beads in the system can be evaluated. These forces are then reduced to the body forces and torques experienced by each knot as mentioned above. Thus, a friction matrix for the system of knots is developed, which may be inverted to yield a diffusion matrix for the system of knots. Using the optical forces experienced by each knot, and the diffusion matrix, the Langevin equation for the system of knots may be integrated using a standard Brownian dynamics approach.[32,33]

2.2 Knot Parameters

The knots shown in Fig. 1 are examples of torus knots, so named because they can be drawn on the surface of a torus without any crossings. The subscripts are indices from the Rolfsen knot table. Torus knots are convenient model knots for simulation because they have a simple chiral rotational symmetry, and because they may be expressed by a simple set of parametric equations:

$$\begin{aligned} x &= ar\cos(p\phi) \\ y &= ar\sin(p\phi) \\ z &= -a\sin(q\phi) \end{aligned} \tag{1}$$

where $r = cos(q\phi) + c$ and $0 < \phi < 2\pi$. p and q are prime numbers that define the knot, while c is a constant that sets the radius of the torus, and a is a scale factor which depends on the size and number of beads used i.e. the contour length of the knotted nanowire. In practice, a set of unevenly spaced values of ϕ are required to obtain equally spaced and non-overlapping beads.

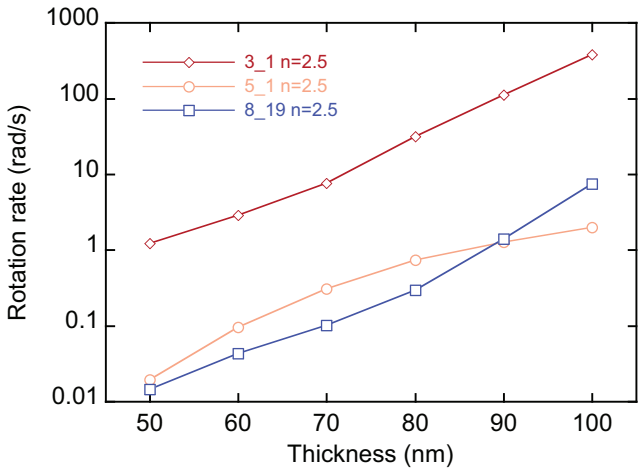

Figure 2. The rotation rates of knots of type 3_1, 5_1 and 8_{19} in counter-propagating circularly polarised plane waves.

The parameters used to define the 3_1, 5_1 and 8_{19} knots are shown in Table 1. c was nominally set to 2 units, but had to be increased slightly for the 5_1 and 8_{19} knots to avoid the beads from overlapping each other. All the knots considered all have rotational symmetry and propellor-type chirality.

Knot	p	q	Beads	c
3_1	2	3	30	2.00
5_1	2	5	30	2.15
8_{19}	3	4	32	2.34

Table 1. The parameters used to generate coordinates of knots using Eq. (1).

The simulations consist of either a single knot or a pair of nanowire knots, arranged side-by-side in a single interference fringe of the circularly polarised counter-propagating plane-waves. The knotted nanowires consist of beads of diameter between 50 nm and 100 nm. The contour lengths of the knots range from 1.5 to 3.0 μm, with diameters in the range 0.2 to 0.6 μm depending on the type of knot. A nominal refractive index of 2.5 was used throughout, corresponding to titanium dioxide. The wavelength of the incident counterpropagating waves was 800 nm in vacuum, and the medium was taken as water. The counter-propagating circularly polarised waves have opposite handedness, in order that the electric vectors reinforce at all points during the wave cycle. An intensity of 10 mWμm^{-2} was assumed.

3. RESULTS

3.1 Single Nanowire Knots

As described above, single knots are placed in the plane of a bright interference fringe in the counter-propagating plane waves. It is anticipated that the spin-angular momentum of the circularly polarised waves will interact with the chiral knots, causing them to spin. Figure 2 shows the rotation rates observed for each knot. As might be expected, the rotation rate increases rapidly with the thickness of the knots i.e. with the size of the beads representing them. However, the 3_1 knot shows much greater rotational rates than either the 5_1 or 8_{19}. Also, both left and right handed circularly polarised waves were used, but the rotation rates observed were identical, apart from a change of sign. This was surprising as it was expected that the chirality of, say, a right-handed 3_1 knot would interact differently with either a left or right handed circular polarisation.

The explanation for this behaviour appears to lie with the structure of the knots. Each torus knot has a screw-symmetry. This means it will appear the same when viewed from the perspective of the forward travelling

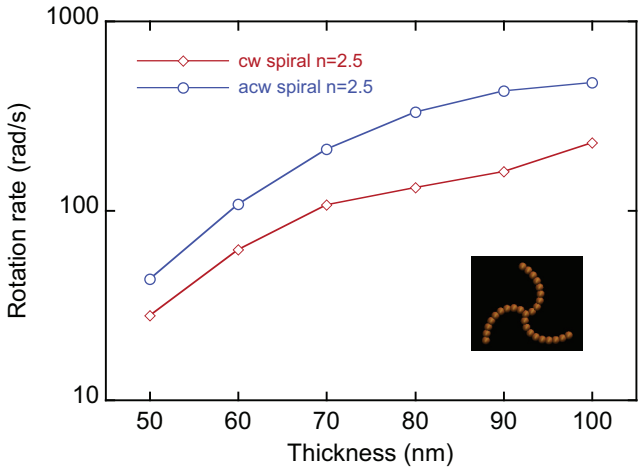

Figure 3. The rotation rates for 3-armed spirals with two different chiralities. The structure is shown in the inset. The modulus of rotation rate is plotted, but the rotation rates for the anti-clockwise spiral (blue trace) should be negative with respect to the clockwise spiral (red trace).

wave or the backward travelling wave. However, as noted in the Methods Section, the two waves have opposite handedness in order to ensure the electric vectors rotate in the same sense. This means that any effects of chirality effectively cancel out. Therefore, the rotation that is observed is not due to the chirality of the knot, but to the non-uniform distribution of matter in the knot. (In optical tweezers, where a single beam is used, this cancellation would not occur and chiral effects should be seen).

The reason for the different rotation rates in the three knots is therefore clear. The 5_1 and 8_{19} knots are compact with little structural variation, and therefore show a weak coupling with the spin-angular momentum of the waves. The 3_1 knot, on the other hand, is more heterogeneous, and therefore shows a greater coupling. The precise details of the rotation rates also depend on the degree of overlap between the knots and the bright interference fringes. This will vary both with knot type and with bead diameter.

To test the hypothesis that the screw nature of the torus knots was preventing their chirality from influencing the rotation rate, a second set of simulations were performed using a 2-dimensional chiral spiral structure. The results are shown in Fig. 3. This time, using left or right handed circularly polarised waves, or equivalently inverting the structure (by flipping the 2-d spiral in the third dimension) resulted in markedly different rotation rates, as expected. Additionally, the rotation rates were generally greater than for the knots, which may be seen to be due to the greater variation in particle density across the structure.

3.2 Binding Between Nanowire Knot Pairs

When pairs of knotted nanowires are placed side-by-side in a single interference fringe, some interesting effects are observed. Firstly, the knots move to a preferred separation, which is generally close to one wavelength of the incident field in the medium. Secondly the knots rotate about an axis perpendicular to the fringe. This was previously observed for single knots, but the rotation rates are different here. Thirdly, the two knots are seen to precess around each other. These results are summarised in Fig. 4 for trefoil (3_1) knot pairs.

On closer inspection, a number of interesting effects are observed. Firstly, as indicated, the binding separation of most knot pairs is approximately one wavelength (around 0.6 μm). However, there is some variation in this. As the knot thickness increases, the binding separation initially decreases, probably as a result of an increased binding interaction, but then increases as it become too large. For knots with a thickness of 90 nm, the separation jumps to a new value of around 0.8 μm.

For the smaller knots, the rotation and precession of the knots are in opposite senses. In particular, for the 50 nm and 60 nm nanowire knots, the rotation and precession are equal and opposite. In practical terms, this

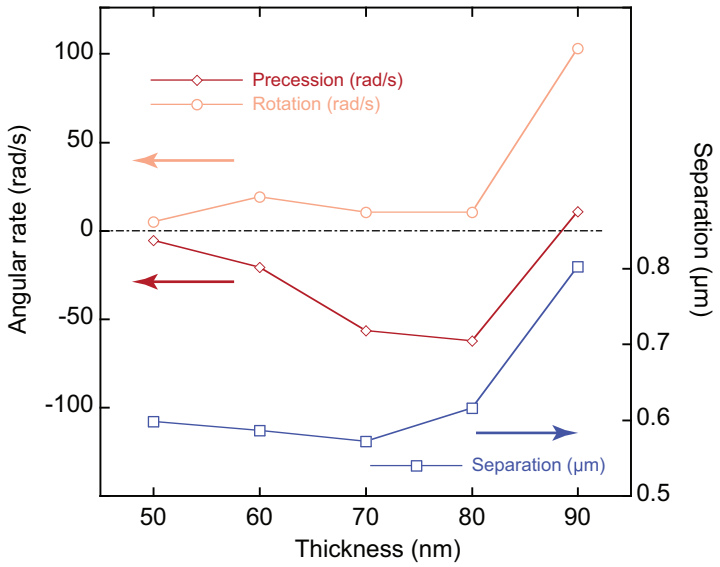

Figure 4. Rotation and precession rates, and binding separations, for pairs of 3_1 knots of various thicknesses.

implies that the two knots have assumed a fixed orientation with respect to each other, and are rotating as a rigid body. We may say that the particles are bound both positionally and orientationally. The particular configuration that is favoured in these cases is for two edges, of the approximately triangular knots, to face each other.

For the 70 nm and 80 nm knots, the rotation and precession appear to become decoupled. The precession rate continuous to increase with knot thickness, but the rotation rates become approximately constant. The most unexpected effect is that, for the 90 nm particles, the precession rate reverses, so that the pair of particles precess in the same sense that they rotate. Simultaneously, the binding separation increases, and the rotation rate increases towards that of an isolated particle. A similar behaviour has been observed for cinquefoil (5_1) knot pairs (not shown).

4. DISCUSSION

Brownian dynamics simulations have been performed on individual and pairs of nanowire knots in circularly polarised counter-propagating plane waves. The knots were chosen partly as model chiral particles which were relatively easy to construct, but also partly because of an increase in interest in the physical applications of knots. As expected, individual knot particles rotated in the circularly polarised beams, with the optical spin angular momentum of the incident waves coupling to the mechanical spin of the particles. However, the chirality of the knots was found not to have a role in this angular momentum transfer, due to the symmetry of the counter-propagating beams.

Pairs of knots are found to bind together optically, at a separation which is typically close to the wavelength of light in the medium surrounding the particles. Interestingly, the pairs of knots precess about each other, while also spinning. In other words they acquire both spin and orbital angular momentum from the optical field. While vortex beams exist, which can transport both spin and orbital optical angular momentum,[34–36] the nature of the plane wave is that it can only ever carry spin angular momentum. The coupling that is occurring, between the spin optical angular momentum of the field and the orbital angular momentum of the particles, is mediated by the strong binding interaction between the particle pairs.

For smaller knots, the spin-coupling from the optical field is relatively weak, and the particle orientation is dominated by the orientational binding between the particle pairs. However, as the particle size increases, the spin-coupling becomes much stronger so that, for the largest knots simulated, the spin-rotation rate is almost the

same as for isolated particles, and is unaffected by the binding. Most intriguingly, the spin-orbit coupling that occurs is seen to change sign for the largest knots simulated. It is not clear at this point whether this reversal is due to the size of the particles, or to their separation, and this is the subject of further study.

Additional simulations have been performed (not shown here), examining larger clusters of nanowire knot particles. The general finding is that the particles cluster in hexagonal arrays, with a lattice spacings on the order of a wavelength. Both spin and orbital motion are observed.

The computational method employed incorporates a full optical and hydrodynamic calculation in a Brownian dynamics simulation. The nanowire knots are minimally represented by a single line of spheres, constrained to move as rigid bodies; the nanowire thickness corresponds to the sphere diameters employed. Improvements to the model would involve using more beads, or cells, to represent the knots, but this would come at the expense of an increased computational burden. One possible way to improve the realism would be to use different resolutions: a fine discretization for the optical problem, and a coarser approach for the hydrodynamic problem. This is the subject of ongoing efforts.

ACKNOWLEDGMENTS

The authors thank ISI Brno for financial support for S.H.S. and the University of Bristol Advanced Computing Research Centre (`http://acrc.bris.ac.uk/`) for provision of computing resources. This research was funded by a Leverhulme Trust Research Programme Grant.

REFERENCES

[1] Burns, M. M., Fournier, J.-M., and Golovchenko, J. A., "Optical binding," *Phys. Rev. Lett.* **63**, 1233 (1989).

[2] Singer, W., Frick, M., Bernet, S., and Ritsch-Marte, M., "Self-organized array of regularly spaced microbeads in a fiber-optical trap," *JOSA B* **20**, 1568–1574 (2003).

[3] Taylor, J. M. and Love, G. D., "Spontaneous symmetry breaking and circulation by optically bound microparticle chains in gaussian beam traps," *Phys. Rev. A* **80**, 053808 (2009).

[4] Karásek, V., Brzobohatỳ, O., and Zemánek, P., "Longitudinal optical binding of several spherical particles studied by the coupled dipole method," *Journal of Optics A: Pure and Applied Optics* **11**, 034009 (2009).

[5] Metzger, N. K., Dholakia, K., and Wright, E. M., "Observation of bistability and hysteresis in optical binding of two dielectric spheres," *Phys. Rev. Lett.* **96**, 068102 (2006).

[6] Čižmár, T., Romero, L. C. D., Dholakia, K., and Andrews, D. L., "Multiple optical trapping and binding: new routes to self-assembly," *J. Phys. B: Atomic, Molecular and Optical Physics* **43**, 102001 (2010).

[7] Demergis, V. and Florin, E.-L., "Ultrastrong optical binding of metallic nanoparticles," *Nano Letters* **12**(11), 5756–5760 (2012).

[8] Yan, Z., Shah, R. A., Chado, G., Gray, S. K., Pelton, M., and Scherer, N. F., "Guiding spatial arrangements of silver nanoparticles by optical binding interactions in shaped light fields," *ACS Nano* **7**(2), 1790–1802 (2013).

[9] Nome, R. A., Guffey, M. J., Scherer, N. F., and Gray, S. K., "Plasmonic interactions and optical forces between au bipyramidal nanoparticle dimers," *J. Phys. Chem. A* **113**, 4408–4415 (2009).

[10] Andrews, D. L. and Bradshaw, D. S., "Laser-induced forces between carbon nanotubes," *Optics Letters* **30**(7), 783–785 (2005).

[11] Simpson, S. H. and Hanna, S., "First-order nonconservative motion of optically trapped nonspherical particles," *Phys. Rev. E* **82**(3, 1), 031141 (2010).

[12] Irrera, A., Artoni, P., Saija, R., Gucciardi, P. G., Iatì, M. A., Borghese, F., Denti, P., Iacona, F., Priolo, F., and Maragò, O. M., "Size-scaling in optical trapping of silicon nanowires," *Nano Lett.* **11**, 4879–4884 (2011).

[13] Maragó, O. M., Bonaccorso, F., Saija, R., Privitera, G., Gucciardi, P. G., Iatì, M. A., Calogero, G., Jones, P. H., Borghese, F., Denti, P., et al., "Brownian motion of graphene," *ACS Nano* **4**, 7515–7523 (2010).

[14] Ridolfo, A., Saija, R., Savasta, S., Jones, P. H., Iatì, M. A., and Marago, O. M., "Fano-doppler laser cooling of hybrid nanostructures," *ACS Nano* **5**, 7354–7361 (2011).

[15] Wang, F., Toe, W. J., Lee, W. M., McGloin, D., Gao, Q., Tan, H. H., Jagadish, C., and Reece, P. J., "Resolving stable axial trapping points of nanowires in an optical tweezers using photoluminescence mapping," *Nano Lett.* **13**, 1185–1191 (2013).

[16] Reece, P. J., Toe, W. J., Wang, F., Paiman, S., Gao, Q., Tan, H. H., and Jagadish, C., "Characterization of semiconductor nanowires using optical tweezers," *Nano Lett.* **11**, 2375–2381 (2011).

[17] Phillips, D. B., Carberry, D. M., Simpson, S. H., Schaefer, H., Steinhart, M., Bowman, R., Gibson, G. M., Padgett, M. J., Hanna, S., and Miles, M. J., "Optimizing the optical trapping stiffness of holographically trapped microrods using high-speed video tracking," *J. Optics* **13**, 044023 (2011).

[18] Cölfen, H. and Mann, S., "Higher-order organization by mesoscale self-assembly and transformation of hybrid nanostructures," *Angewandte Chemie International Edition* **42**(21), 2350–2365 (2003).

[19] Mann, S., "Self-assembly and transformation of hybrid nano-objects and nanostructures under equilibrium and non-equilibrium conditions," *Nature Materials* **8**(10), 781–792 (2009).

[20] Taylor, W. R., "A deeply knotted protein structure and how it might fold," *Nature* **406**, 916–919 (2000).

[21] Virnau, P., Mirny, L. A., and Kardar, M., "Intricate knots in proteins: Function and evolution," *PLOS Comp. Biol.* **2**, 1074–1079 (2006).

[22] Arsuaga, J., Vazquez, M., Trigueros, S., Sumners, D., and Roca, J., "Knotting probability of DNA molecules confined in restricted volumes: DNA knotting in phage capsids," *PNAS* **99**, 5373–5377 (2002).

[23] Arsuaga, J., Vazquez, M., McGuirk, P., Trigueros, S., Sumners, D. W., and Roca, J., "DNA knots reveal a chiral organization of DNA in phage capsids," *PNAS* **102**, 9165–9169 (2005).

[24] Staczek, P. and Higgins, N. P., "Gyrase and Topo IV modulate chromosome domain size in vivo," *Molecular Microbiol.* **29**, 1435–1448 (1998).

[25] Dennis, M. R., King, R. P., Jack, B., O/'Holleran, K., and Padgett, M. J., "Isolated optical vortex knots," *Nat. Phys.* **6**, 118–121 (2010).

[26] Taylor, A. J. and Dennis, M. R., "Vortex knots in tangled quantum eigenfunctions," *Nat. Commun.* **7**, 12346 (2016).

[27] Hall, D. S., Ray, M. W., Tiurev, K., Ruokokoski, E., Gheorghe, A. H., and Mottonen, M., "Tying quantum knots," *Nat Phys* **12**, 478–483 (05 2016).

[28] Yurkin, M. A., Maltsev, V. P., and Hoekstra, A. G., "The discrete dipole approximation for simulation of light scattering by particles much larger than the wavelength," *JQSRT* **106**, 546–557 (2007).

[29] Simpson, S. H. and Hanna, S., "Application of the discrete dipole approximation to optical trapping calculations of inhomogeneous and anisotropic particles," *Optics Express* **19**(17), 16526–16541 (2011).

[30] Simpson, S. H., Phillips, D., Carberry, D., and Hanna, S., "Bespoke optical springs and passive force clamps from shaped dielectric particles," *JQSRT* **126**, 91–98 (2013).

[31] Happel, J. and Brenner, H., [*Low Reynolds number hydrodynamics: with special applications to particulate media*], vol. 1, Springer (1965).

[32] Ermak, D. L. and McCammon, J., "Brownian dynamics with hydrodynamic interactions," *The Journal of chemical physics* **69**, 1352 (1978).

[33] Brady, J. F. and Bossis, G., "Stokesian dynamics," *Annual Review of Fluid Mechanics* **20**, 111–157 (1988).

[34] Simpson, S. H. and Hanna, S., "Rotation of absorbing spheres in Laguerre-Gaussian beams," *JOSA A* **26**, 173–183 (2009).

[35] Simpson, S. H. and Hanna, S., "Optical angular momentum transfer by Laguerre-Gaussian beams," *JOSA A* **26**, 625–638 (2009).

[36] Simpson, S. H. and Hanna, S., "Orbital motion of optically trapped particles in Laguerre-Gaussian beams," *JOSA A* **27**, 2061–2071 (2010).